PERGAMON

Chemical Engineering Science 56 (2001) 1631–1638

Chemical Engineering Science

www.elsevier.nl/locate/ces

# Modeling of a fluidized-bed photocatalytic reactor for water pollution abatement

M. G. Chiovetta, R. L. Romero, A. E. Cassano*

*INTEC, Instituto de Desarrollo Tecnológico para la Industria Química, Univ. Nac. Litoral-CONICET Güemes 3450, 3000 Santa Fe, Argentina*

**Abstract**

A system consisting of a fluidized bed of quartz-support particles impregnated with titanium dioxide in a UV-irradiated annular arrangement is presented as an efficient reactor configuration for the photocatalytic oxidation of diluted trichloroethylene in water. A mathematical scheme is developed to analyze the fluidized bed, including a detailed radiation field representation and an intrinsic kinetic scheme. The model is used to predict operating conditions at which good mixing states and fluid renewal rates are accomplished throughout the bed, and to compute contaminant decay. Systems analyzed include a high-pressure Hg lamp, 0.3 m long setup, and an "actinic", low-pressure lamp in a 1 m long reactor. For relatively high flow rates, per-pass oxidation conversions between 9 and 35% are reached depending on the reactor system considered, and on the titanium oxide concentration in the bed, ranging between 0.1 and 0.5 kg $m^{-3}$. Results indicate a strong dependence of reactor performance upon the radiation energy available at each point in the annulus. This availability, in turn, is a fraction of both lamp power and UV-radiation penetration within the bed. For the selected contaminant, the kinetic scheme shows that the low-energy disadvantage in the low-pressure lamp reactor can be compensated by the fact that the radiation field is more evenly distributed throughout the fluidized particle bed. 

*Keywords:* Photocatalytic reactor; Fluidized bed; Titanium dioxide; Photocatalytic oxidation; Mathematical model; Trichloroethylene abatement

## 1. Introduction

A continuous device for the lodging of a fluid medium where efficient photo-catalytic oxidation of contaminants using $TiO_2$ in its anatase form and UV radiation takes place must solve some typical problems

(a) The catalyst should not be lost to the exiting stream, in spite of titanium oxide particle sizes in the order of 20/200 nm.
(b) The contaminants are present in low concentrations, usually in the range of 10–100 ppm, creating a reaction environment subject to possible transport limitations.
(c) UV-radiation activation is required, demanding a configuration able to guarantee the illumination of the active sites in as much of the whole reaction environment as possible.
(d) The titanium oxide is a highly absorbing material; catalyst concentration and reactor geometry must be adjusted to permit UV light to reach the largest reactor volume before becoming fully absorbed, and, at the same time, to enable a high fluid-renewal rate.

A fluidized bed with quartz support particles impregnated with titanium oxide is a reasonable reactor alternative. At the proper flow regimes, good mixing conditions are ensured throughout the bed, thus producing high renewal rates for the fluid in the annulus regions closer to the UV source, where the radiation field is stronger. Catalyst particles are fixed in a quartz-sand bed from which only a small titanium oxide fraction could be lost by attrition or disengagement from the bed and needs recovery.

In what follows, the fluidized bed is analyzed by means of a mathematical model used to predict proper operating conditions and oxidation performance. Two reactor schemes are modeled, one for a high-pressure, high-energy UV lamp, typical of an experimental setup, and a second for a low-pressure, low-energy actinic lamp, more likely to be used, for price and simplicity of operation, in an application device. The model presented is used to calculate fluidization conditions that ensure good

*Corresponding author: Tel.: +54-342-455-9175; fax: +54-342-455-9185.

*E-mail address:* acassano@alpha.arcride.edu.ar (A. E. Cassano).

0009-2509/01/$ - see front matter 
PII: S0009-2509(00)00391-2

mixing across the annulus, and to predict conversions for the oxidation of a stream of low concentration trichloroethylene in water; various $TiO_2$ concentrations in the bed are modeled.

## 2. The system modeled

### 2.1. Particle and reactor description

The catalyst is Aldrich $TiO_2$ (anatase) in the form of a fine powder of spherical particles. The catalyst particle-size-range is 150 to 200 nm, with an average diameter of 175 nm; its density is 3800 kg/m$^3$. The selected support is quartz, due to its UV-conducting nature, in the form of sphere-like particles with a size range between 212 and 297 μm, with an average diameter 270 μm and a 2650 kg/m$^3$ density; the model assumes that they are solid, smooth-surface spheres.

Various amounts of $TiO_2$ immobilized on the support particle produce a combined support-catalyst particle in which, at most, a nominal single layer of catalyst particles is assumed to fully cover the external surface of the support. The degree of surface covering (%) is used as an adjusting variable to control the overall titanium dioxide concentration in the fluidized bed. This percentage has an impact on both illumination and reactor performance, as shown later. In terms of the fluidization condition, it is worth noticing that the deposit will produce a diameter change in the order of 0.126%, that can be neglected for the purpose of considering the dynamic conditions of the particles in the bed.

Simulations are conducted for concentration of $TiO_2$ in the bed ranging from 0.1 to 0.5 kg/m$^3$, the upper limit being imposed mostly by radiation field decay along the radial coordinate.

Two UV lamps are modeled, in turn leading to two reactor-system configurations termed Reactors 1 and 2, respectively. Each consists of a pair of concentric Pyrex–Duran/Schott borosilicate glass tubes. The interior tube is transparent to UV radiation, since the lamp is placed at the axial center of symmetry of the configuration, as schematically shown in Fig. 1. Fluid entrance is performed via a bottom-end distribution system to produce a reasonable azimuthal distribution of the flow entering the annular region between the concentric tubes. The concentric-tube geometry determines a reaction volumetric cell, typical of an annular symmetry, with an elementary volume as a function of the radius $r$ and height $h$ being entered by a liquid mass flow rate $F$ at any reactor point, as schematically depicted in Fig. 2.

Reactor 1 is built with tubes with a wall thickness of 0.0025 m, and internal diameters of 0.065 and 0.1 m, respectively. They house a 0.3 m long Hanovia LL-189a-10/1200 lamp. The illuminated height in the annular reaction zone is 0.30 m.

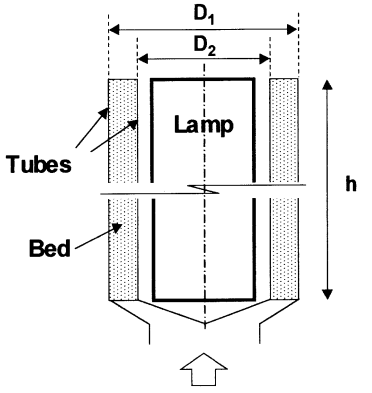


Fig. 1. Fluidized bed reactor scheme, valid for both Reactors 1 and 2.

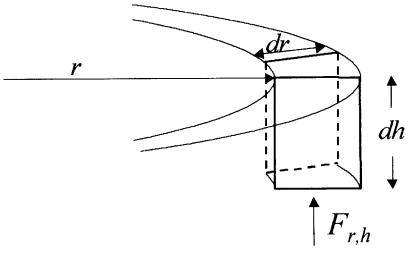


Fig. 2. Volumetric-cell scheme, showing main variables for local kinetic calculations.

Reactor 2 consists of a set of 0.0025 m wall-thickness concentric tubes with internal diameters of 0.065 and 0.085 m, respectively. The lamp in this system is a 1.5 m long Phillips TL 80W/09 N actinic lamp. The illuminated height in the annular reaction zone of Reactor 2 is 1.0 m.

### 2.2. Fluid dynamic conditions

In fluidized, liquid–solid beds, typical expressions to analyze the fluidization conditions for spherical particles are the Kozeny, and the Ergun equations (Coulson, Richardson, Backhurst & Harter, 1978). Since particles are fairly spherical, the Kozeny equation may be found to be producing conservative values for the minimum-fluidization fluid velocity. However, for the conditions studied, predictions from both equations are remarkably close. Hence, in this work Ergun's expression is used to compute the minimum fluidization velocity $u_{mf}$ as a function of bed parameters and the minimum fluidization void-fraction $e_{mf}$:

$$u_{mf} = 42.86\frac{\mu}{\mathrm{d}\rho}(1-e_{mf})\left[\sqrt{1+3.11\times10^{-4}Ga\frac{e_{mf}^3}{(1-e_{mf})^2}}-1\right],$$

$$Ga=\frac{\rho g d^3(\rho_s-\rho)}{\mu^2}. \quad (1)$$

The initial situation for the bed is that of a packed bed of approximately equal-size support spheres located at the bottom of the reactor prior to any liquid flow entering the vessel. The initial void fraction can be obtained from random packing models; the problem has been discussed by Bernal (1959), and Gotoh (1977) with both theoretical and experimental analyses for the random packing of spheres in a cylindrical container. Here, the most likely values for the void fractions are between 0.36 and 0.44, depending on the ratio of particle to cylinder values. Since the support particle-size distribution is narrow, the initial bed (i.e. the set of particles placed inside the reactor at the beginning of the process) can be considered ordered, and thus attaining an initial void fraction $e_0$ approximately equal to 0.4. For the same reason, the bed-packing arrangement is considered unchanged during all flow conditions when fluid velocity $u$ is below $u_{mf}$. Hence, $e_{mf} = e_0 = e_{u0} = 0.4$.

The expansion of the bed as fluid velocity increases above the minimum fluidization conditions is calculated using Richardson and Zaki's (1954) equation for void fraction of the bed $e$. The expression uses $u_i$, a terminal velocity corrected for the distance $d_t$ between the cylindrical, walls as follows:

$$\frac{u}{u_i} = e^n, \quad \log_{10} u_i = \log_{10} u_0 - \frac{d}{d_t}, \quad n = \frac{\log(u_{mf}/u_i)}{\log(e_{mf})}. \quad (2)$$

The terminal Reynolds number $Re_0$ is used to calculate the terminal velocity for a support particle, as a function of the Galileo number using Khan and Richardson's (1990) expression:

$$Ga = (2.07e^{-0.27n} + 0.33Re_0^{0.37}e^{-0.64n})^{3.45}Re_0^{0.93},$$

$$Re_0 = d\rho u_0 \mu^{-1}, \quad 3.6 < Ga < 10^5. \quad (3)$$

For the average support-catalyst particle diameter is 2.1 and the water–trichloroethylene fluid the value of the Galileo number is 318.27. Solving for $Re_0$ (270 μm average, single particle), a value of 10.08 is obtained. The corresponding terminal velocity $u_0$ is 0.0370 m/s. In the case of the smallest support particle (212 μm), the predicted terminal velocity would be $u_0 = 0.026$ m/s. One important parameter for the bed, usually termed velocity number $V_e$, is the ratio between the fluid velocity $u$ and $u_{mf}$. A particular value $V_{e0}$ computed for a single-particle terminal velocity settles the bed operating window, since the bed should be fluidized ($V_e > 1$) but must not loose particles ($V_e < V_{e0}$). Ergun's prediction for $e_{mf} = 0.40$ gives $u_{mf} = 0.00083$ m/s, while $V_{e0}$ is in the order of 46, from Eq. (3). Using the experimental and theoretical data of Rowe, Rowe and partridge, and Goddard and Richardson compiled in a graph of $u_0/u_{mf}$ by Coulson et al. (1978), the later value of $V_{e0} \approx 46$ proves adequate. From the said data, the regime for the expected fluidized bed is in an intermediate region between the low and high Galileo numbers (with corresponding $V_{e0} \approx 80$ and $\approx 10$, respectively). Hence, the reactors modeled can operate in a particulate, fairly strong fluidization region (for instance $V_e \approx 15$ to 30) and still away from the drag condition that may take the particles with the exiting flow.

## 3. Radiation field modeling

Radiation fields in the bed are calculated for each catalyst concentration, using the complete set of data and an isotropic-scattering model (Brandi, Alfano & Cassano, 1999) for the suspended Aldrich titanium oxide system in Romero, Alfano and Cassano (1997). The resulting predictions for the case of 0.1 kg/m$^3$ of catalyst in the bed for Reactors 1 and 2 are presented in Figs. 3(a) and (b), respectively. Curves for the rate of photon absorption $E_a$ are shown as functions of the radial position in the annulus. Profiles are shown for the bottom of the reactor ($h = 0$), the center of the reactor height (0.15 and 0.5 m, respectively) and a relevant intermediate height for each reactor.

The radiation-field model computes the rate of photon absorption at any position within the reaction annulus as a function of both reactor height and radius for any given amount of titanium oxide per unit reaction volume. The integro-differential equation solving the annulus field are solved using the discrete-ordinate method to produce the local volumetric rate of energy absorption (LVREA) distribution at each volume cell within the annulus. Since, the problem deals with a catalytic reaction with no energy absorption by the fluid, the absorbed radiation field is independent of the reaction extent. Simulations were performed for all catalyst concentrations using two schemes according to the phase function for the radiation distribution: (a) the isotropic-scattering model, with uniform scattering in all directions; and (b) the diffuse-reflection model, which has a smooth anisotropy and significant back scattering. In this work, only the isotropic model predictions are shown.

The radiation field thus calculated for a titanium oxide suspension in water is used as the available LVREA for the supported titanium oxide particles in a fluidized bed with the same resulting catalyst concentration. The fluidized-bed reactor is considered as behaving in an equivalent fashion energy-wise as the corresponding suspended titanium oxide reactor. The equivalence is a reasonably valid approximation since (a) quartz particles perform as a rather poorly absorbing medium in terms of UV-light handling, and (b) good fluidization conditions imply bed porosities in the 0.7 to 0.9 range. The latter allows the distance between titanium oxide elementary particles to be in the same order as that found in a dilute suspension.

The radial profiles in Fig. 3 indicate a strong absorption for low values of $r$. Almost exponential decays are

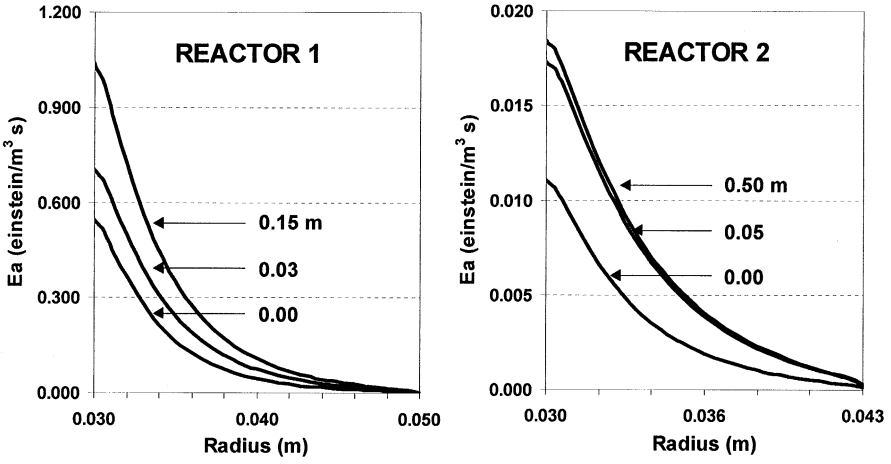


Fig. 3. (a) UV-field $E_a$ (einstein/m$^3$s) vs. annulus radius (m), for various heights from the bottom, Reactor 1. 0.1 kg/m$^3$ catalyst. (b) UV-field $E_a$ (einstein/m$^3$s) vs. annulus radius (m), for various heights from the bottom, Reactor 2. 0.1 kg/m$^3$ catalyst.

observed along the radius, save a region very close to the inner wall were in-scattering contributions alter the domination of the absorption phenomena. When comparing Reactors 1 and 2, the difference in lamp intensity becomes apparent both in the $y$-axis scale and in the radial distribution. Since $TiO_2$ is a highly UV-absorbing material, the plot for Reactor 1 shows a much stronger decay; particles located close to the inner wall absorb much of the usable energy, thus proportionally diminishing its availability deeper in the annulus. Profiles in Reactor 2 depict a more uniform distribution of available radiation energy in the radial coordinate. For the 0.1 kg/m$^3$ case shown in Fig. 3, at the reactor-height center, the ratio between Ea at the radial center of the annulus and $E_a$ at the inner radius is 0.10 for Reactor 1 and 0.22 for Reactor 2. The figures become 0.0074 for Reactor 1 and 0.03 for Reactor 2 when the $E_a$ ratio between the outermost and innermost radial points are compared. This numbers indicate a 2.2- and 4-fold relative decrease of the available energy at the annulus-center and at the external radius, respectively, when Reactors 1 and 2 are compared. This fact is important in terms of overall oxidation performance since, in Reactor 2, larger portions of the bed will still have relatively high available energy, when compared to those at the innermost radial points.

With regard to the axial position, at the reactor top (and bottom) ends the profiles show a significant although different decrease in $E_a$ produced by the characteristics of the irradiating boundary conditions in Reactors 1 and 2 (lamp-end effects). In the former, the curve for $h = 0.03$ m (10% of the reactor height) still shows the effect of a lamp with the same length as the reactor's. For Reactor 2, the curve for $h = 0.1$ m (10% of the reactor height) is not shown because it runs almost superimposed with that for $h = 0.5$ m. Instead, the $h = 0.05$ m curve (5% of the reactor height) shows a distribution almost identical to that at the center. Again, also in the axial direction Reactor 2 shows a more evenly distributed radiation field; the reason is the change in the axial boundary condition associated with the different length of lamp (1.5 m) and reactor (1 m).

## 4. Reaction modeling

Mass balances for the contaminant are performed as functions of bed- height using the kinetic model in Alfano, Cabrera and Cassano (1997) and Cabrera, Alfano and Cassano (1997). The model is able to represent the time evolution of the photocatalytic oxidation of trichloroethylene in water via hydroxyl radical attack for the initiation of the reaction, when catalyst particles in contact with the contaminant in water are activated by UV radiation. Oxygen is considered present in excess in the reacting medium. No mass transport limitations are assumed for the contaminant in the liquid phase. No homogeneous oxidation is considered within the fluid phase because TCE is transparent in the employed wavelength range. For proper velocities, such as those in the $15–30V_e$ range selected in Section 2.2, good mixing conditions result from the fluidized-bed operation. Infrared radiation is filtered out and reaction heat is negligible; hence, isothermal behavior can be safely assumed.

For the various catalyst concentrations in the bed, and the corresponding radiation-field distributions in Section 3 above, the intrinsic kinetics expressions are used locally to calculate the oxidation rate at the supported titanium dioxide active sites located at any given point in the reactor bed. The elementary fluidized bed volume in Fig. 2 is selected considering cylindrical symmetry for each radius $r$ and heigh $h$:

$$dV_r = 2\pi r\, dr\, dh. \quad (4)$$

The contaminant flux at any given $h$ and $r$ within the annulus in kg mol $s^{-1}$ is

$$F_{rh} = F_{rh+dh} + r_v\,dV_r = F_{rh} + dF_{rh} + r_v\,dV_r. \quad (5)$$

Negligible axial and radial diffusion effects in the bed are assumed, since only velocity numbers exceeding of 15 are used. The contaminant flux change resulting from oxidation is a function of the photo-catalytic reaction in the elementary volume in Eq. (4):

$$dF_{rh} = -r_v(r,h)\,dV_r = -r_a a_s C_{mp} 2\pi r\,dr\,dh. \quad (6)$$

The kinetic expression in Alfano et al. (1997) is used to solve for $r_a$, the contaminant oxidation rate at the titanium oxide particle surface in $dV_r$, in kg mol $m_{cat}^{-2}$ $s^{-1}$, with $C_i$ the contaminant concentration in $dV_r$:

$$r_a = k_1\left\{-\frac{K_i C_i(r,h)}{1+K_i C_i(r,h)} + \sqrt{\left(\frac{K_i C_i(r,h)}{1+K_i C_i(r,h)}\right)^2 + \frac{k_2 E_a(r,h)}{C_{mp}}}\right\}. \quad (7)$$

Once the contaminant-flux decay is obtained for each $dV_r(r,h)$, the contaminant concentration is averaged using rigorous integration throughout the radial coordinate at any given $h$ to account for highly mixed state of the bed.

Subsequent integration of the $F$ along the water path (the $h$ coordinate) renders the contaminant flux as a function of the bed height. Oxygen concentration and temperature are assumed to be uniform and constant. Since contaminant concentrations must be calculated for each height as a function of local reacting conditions (namely the concentration itself and the radiation field) an iterative numerical scheme is used to solve for the resulting integral equations.

## 5. Simulation results

### 5.1. Contaminant concentration profile

In order to process the fluid dynamics, radiation field and kinetic superimposed schemes in Sections 2–4 above, firstly the fluidized-bed operating conditions are determined. In order to assure good mixing conditions, velocity numbers in the 15–30 range are chosen.

Firstly, with the known average diameter and density of the quartz particles, and the fluid properties (density, viscosity), the minimum fluidization velocity is calculated using Eq. (1). Then, the terminal (escape) velocity for the smaller quartz particle in the distribution (212 μm) is computed using Eq. (3). Now, a $V_e$ is selected in the range above, thus fixing the value of the fluid velocity $u$, which is checked to guarantee that is lower than the single-particle escape velocity. The bed expansion index is calculated next with Eq. (2) to determine the bed porosity and the support solid fraction. Since each reactor has a given illuminated height, for each $V_e$ and reactor only one initial support mass will expand to reach the bed void fraction that fills the illuminated bed height. This support mass is calculated using the dimensions of the bed for each reactor and the recently obtained bed void-fraction. Finally, the support-coverage percentage required to render each of the selected catalyst concentrations is determined for the corresponding $V_e$.

A summary of the values resulting when the procedure in the paragraph above is applied is presented in Table 1 for various $V_e$. The amount of support decreases as expected with $V_e$, since higher fluid velocities produce larger bed expansions, thus generating higher void fractions and, hence, smaller amounts of support in a bed height equal to the illuminated region. Cover percentages are in all cases below 100%.

With the fluidized-bed conditions settled, the radiation field in Section 3 is employed with the kinetics expressions in Section 4 to calculate the contaminant concentration variation as the fluid moves through the bed. Constants for the kinetic expression in Eq. (7) for trichloroethylene and Aldrich $TiO_2$ are taken from Cabrera et al. (1997). The values are presented in Table 2.

A set of typical oxidation results predicted by the model is shown in Figs. 4(a) and (b). The percentage of the entering Trichloroethylene concentration is shown as a function of the percent of the reactor height for both Reactors 1 and 2, respectively. The system was simulated with a $V_e = 30$ and the kinetic parameters in Table 2. Results are computed for three catalyst concentrations in the bed.

Table 1
Fluidized-bed operating conditions for various $V_e$ (for Reactor 2)

| $V_e$ | $u$ (m/s) | $u_{mf}$ (m/s) | $u_0$ (m/s) | Bed void-fraction | Support mass (kg) | Percentage of support coverage | | |
|---|---|---|---|---|---|---|---|---|
| | | | | | | 0.1 kg/m$^3$ | 0.3 kg/m$^3$ | 0.5 kg/m$^3$ |
| 15 | 0.013 | 0.00083 | 0.037 | 0.77 | 1.706 | 6 | 17 | 23 |
| 20 | 0.017 | 0.00083 | 0.037 | 0.83 | 1.282 | 8 | 23 | 30 |
| 25 | 0.020 | 0.00083 | 0.037 | 0.88 | 0.933 | 11 | 32 | 52 |
| 30 | 0.025 | 0.00083 | 0.037 | 0.91 | 0.632 | 16 | 44 | 62 |

Table 2
Kinetic parameters and variables

| Symbol | Description | Value | Units |
|---|---|---|---|
| $C_i^0$ | Trichloroethylene concentration entering the bed | $1 \times 10^{-4}$ | kg mol m$^{-3}$ |
| $C_{mp}$ | Titanium dioxide concentration in the bed | 0.1 to 0.5 | kg m$^{-3}$ |
| $K_i$ | Kinetic parameter in Eq. (4) from Cabrera et al. (1997) | $6.42 \times 10^3$ | m$^3$ kg mol$^{-1}$ |
| $k_1$ | Kinetic parameter in Eq. (4) from Cabrera et al. (1997) | $2.46 \times 10^{-13}$ | kg mol s$^{-1}$ m$^{-2}$ |
| $k_2$ | Kinetic parameter in Eq. (4) from Cabrera et al. (1997) | $1.57 \times 10^8$ | kg s einstein$^{-1}$ |
| $a_s$ | Titanium oxide particle specific surface area | $9.6 \times 10^3$ | m$^2$ kg$^{-1}$ |

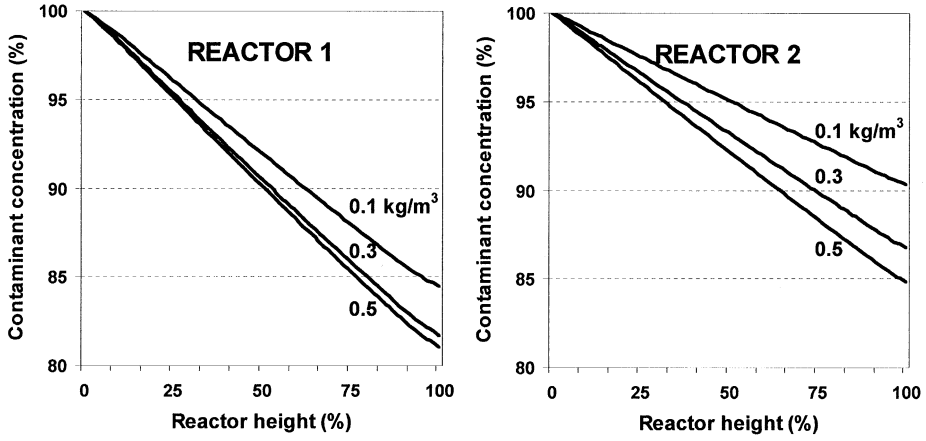


Fig. 4. (a) Contaminant concentration (%) vs. reactor height (%), for various catalyst concentrations, Reactor 1, $V_e = 30$. (b) Contaminant concentration (%) vs. reactor height (%), for various catalyst concentrations, Reactor 2, $V_e = 30$.

From the analysis of the curves, simulations predict a per-pass substantial decay in trichloroethylene concentration for both reactors. This is particularly important for Reactor 2, since the lamp in this configuration is a relatively cheap, low power-consumption lamp. Per-pass conversions obtained for Reactor 2 for the 0.1, 0.3, and 0.5 kg/m$^3$ catalyst concentrations are, respectively, 9.68, 13.22 and 15.19%. They are in the same order of magnitude of those obtained with the high-energy lamp in Reactor 1: 15.25, 18.29 and 19% for the same set of catalyst concentrations, respectively. Three factors must be considered when analyzing the performance of both configurations: (a) the length of the reactor; (b) the $E_a$ distribution; and (c) the kinetic expression.

To properly effect the comparison, the first element to consider is that the illuminated regions in the reactors are fairly different. Reactor 1 is much shorter than Reactor 2, with a ratio of usable height of 3.33 in favor of the latter. This fact partially offsets the importance of the second factor: The difference in illumination power between the two lamps. As it was indicated in Section 3, the reactor configurations differ not only in their bed height. There is also the fact that the Reactor 2 configuration includes a lamp longer than the illuminated annulus; this length excess attenuates the boundary effect of the UV radiation distribution at the top and bottom end of the bed, thus creating a radiation field more uniform in the axial direction when compared with that in Reactor 1.

With regard to the Ea distribution, there is no single measure to quantify the energy-availability difference, and several concepts must be considered to analyze the importance of this factor. From the plots in Fig. 3, Reactor 1 shows a value for $E_a$ in excess of 1 einstein/m$^3$ s at the innermost point in the bed at the center of the reactor height (1.036 is the precise value). The equivalent figure for Reactor 2 is only of 0.0185, almost 56 times lower. However, when the same comparison is made for the outermost point of the bed radius at the reactor center height, the values are $7.7 \times 10^{-3}$ einstein/m$^3$ s for Reactor 1 and $5.5 \times 10^{-4}$ einstein/m$^3$ s, with a ratio of 13.85. This factor is important since, as it was anticipated in Section 3, the attenuation of the available UV energy in the radial direction is less severe for the low energy lamp system in Reactor 2. This fact makes Reactor 2 reacting cells located at higher radii able to perform an important contribution to the contaminant oxidation process.

The third factor is the form of the oxidation rate expression in Eq. (7) and the manner in which the relative weight of the variables affects its behavior. For the

purpose of its analysis, one can arrange the terms between brackets in Eq. (7) in the form $\gamma = \alpha - (\alpha^2 + \beta)^{1/2}$, where $\alpha = K_i C_i/(1 + K_i C_i)$ and $\beta = k_2 E_a/C_{mp}$. Using the concentration profile and $E_a$ predicted for the 0.3 kg/m$^3$ catalyst concentration in the bed, values of $\alpha$ for both reactors are 0.39 at the bottom and 0.36 at the top. At the top of Reactor 1, $\beta = 6.55 \times 10^8$ for the innermost radial position and $1.33 \times 10^4$ for the outermost. The corresponding figures for $\beta$ in Reactor 2 are $1.74 \times 10^7$ and $6.12 \times 10^3$, respectively. From these values, it is valid to consider that $\gamma = \alpha - (\alpha^2 + \beta)^{1/2}$ is approximately $\gamma \approx \beta^{1/2}$. This form indicates that the kinetic expression at any point in the bed is dominated by the square root of the energy absorption rate $E_a$.

If the values for $\alpha$ and $\beta$ above are used to obtain the ratio of intrinsic, local oxidation rates at the reactor top between Reactors 1 (the most effective) and 2, one obtains for this ratio a value of 6.1 at the innermost radius and 1.5 at the outermost. When an exponential average is computed for this ratio across the radial coordinate, a value slightly higher than 4 is obtained. Basically, this is a representative indicator of the real increase in local oxidation rate between the high-energy and low-energy systems for the conditions considered. Since the residence time is 3.3 larger for Reactor 2, the net overall effect in per-pass conversation should favor Reactor 1 (4 times more active but 3.3. times shorter) by a factor slightly higher than 1, as shown in the curves in Fig. 4.

Pollutant-decomposition performance for Reactor 2 was compared with that in Cabrera et al. (1997). To reach 10% conversion a residence time of approximately 1 min is required in Reactor 2, while the reactor in the reference, operating in a well-stirred batch mode, would have demanded a residence time of about 10 min.

### 5.2. Fluid velocity effects

The operation of the fluidized bed is highly influenced by the fluid velocity. In this work, care was taken in considering fluid velocities producing velocity numbers in a range guaranteeing good mixing conditions ($V_e > 15$). The results for the oxidation conversion of trichloroethylene when $V_e$ numbers are used within this range are presented in Fig. 5 for both reactors. The plots show the dependence of conversions with residence times, the former being inversely proportional to $V_e$. The results for both reactors reaffirm the analysis in Section 5.1. Reactor 2 behaves in a less effective way in terms of the contaminant oxidation achieved. However, its decrease in overall performance follows the same behavior discussed in the section above for the per-pass conversion, with a net achievement similar to that in Reactor 1.

The impact of $TiO_2$ concentration in the bed, although qualitatively similar in both reactors presents some differences. The curves for 0.5 kg/m$^3$ is closer to the 0.3 one in Reactor 1, indicating a less strong effect of catalyst concentration upon conversion when the former increases. One of the reasons is the square root affecting the value of $C_{mp}$ in the local kinetic expression. However, this fact will not suffice to explain the behavior of the plots when compared with those for Reactor 2, where the curves are more sensitive to catalyst concentration effects.

Analysis of the data again shows the strong impact of the radiation field. For the high-energy lamp, higher concentrations of $TiO_2$ produce less UV-energy availability along the radial direction more rapidly, thus creating a larger region of cells within the bed deprived

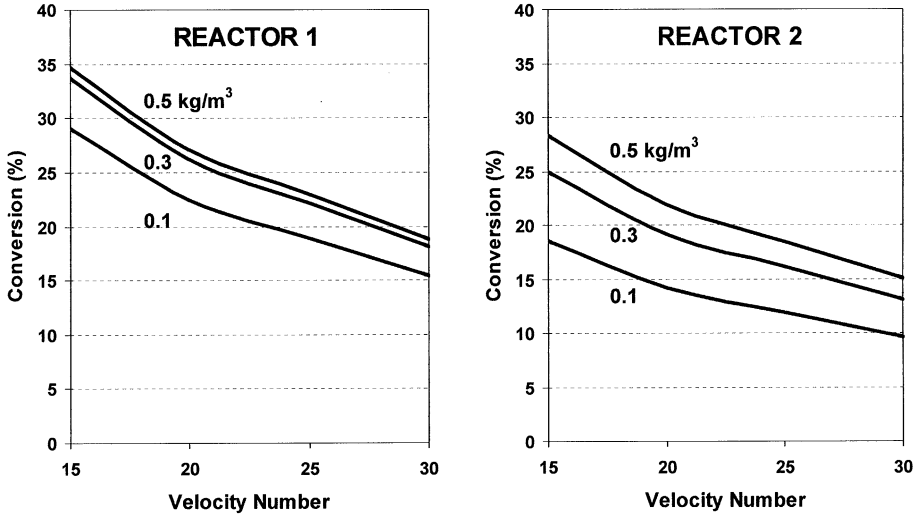


Fig. 5. (a) Conversion (%) vs. velocity number, for various catalyst concentrations, Reactor 1. Conditions as in Tables 1 and 2. (b) Conversion (%) vs. velocity number, for various catalyst concentrations, Reactor 2. Conditions as in Tables 1 and 2.

of proper catalyst photo-activation. The growth in active sites concentration associated with the catalyst concentration increase is not enough to offset the fact that most of the active sites will not have the chance of being illuminated with enough UV radiation.

## 6. Conclusions

The mathematical model developed was used to simulate the behavior of a photocatalytic annular reactor with titanium dioxide as the oxidation catalyst for trichloroethylene contaminated water. Results for high- and low-energy UV lamps were produced to compare both systems. Detailed $E_a$ fields within the bed were used, with rigorous distributions both in the radial and axial directions.

Quartz particles of the studied sizes can be used to establish fluidization conditions without support mass escaping the bed and simultaneously offering good mixing conditions. The said particles can work as an attractive alternative to immobilize small $TiO_2$ particles so as to permit its catalytic activity highly enhanced by UV availability, with the advantage of handling the larger quartz particles, and with negligible downstream catalyst separation.

Energy-distribution effects appear as the dominant factor when considering the oxidation performance, according to predictions. Reasonably high oxidation conversions were obtained for both systems, indicating that a low-energy actinic lamp can be used to reach acceptable per-pass conversions. UV distribution affects the predicted results in a manner suggesting that an even radiation field distribution can help to compensate for lower lamp power.

## Notation

$C_i$ trichloroethylene concentration, kg mol/m$^3$
$d$ quartz, support-particle diameter (μm)
$d_t$ distance between annulus walls, m
$E_a$ rate of energy absorption in Eq. (7), einstein/m$^3$ s.
$e_{mf}$ bed void-fraction at minimum fluidization, dimensionless
$g$ gravity, 9.8 m/s$^2$
$Ga$ galileo number defined in Eq. (2), dimensionless
$h$ axial coordinate, m. In Fig. 1: overall bed height, m
$n$ fluidized-bed expansion index, dimensionless, defined in Eq. (2)
$r$ radial coordinate, m
$Re_0$ reynolds number for a particle at its terminal velocity defined in Eq. (3), dimensionless
$u$ fluid velocity, m/s
$u_0$ terminal velocity for quartz particles, m/s
$u_i$ terminal velocity corrected for wall effects defined in Eq. (2), m/s
$u_{mf}$ minimum-fluidization velocity, m/s
$V$ fluidized bed volume, m$^3$

*Greek letters*
$\mu$ fluid viscosity, 0.001 kg/m s
$\rho$ fluid density, 1000 kg/m$^3$
$\rho_s$ quartz-particle density, 2650 kg/m$^3$

## References

Alfano, O. M., Cabrera, M. I., & Cassano, A. E. (1997). Photocatalytic reactions involving hydroxil radical attack I: reaction kinetics formulation with explicit photo absorption effects. *Journal of Catalysis*, *172*, 370.

Bernal, J.D. (1959). A geometrical approach to the structure of liquids.*Nature* (London), 183, 141.

Brandi, R. J., Alfano, O. M., & Cassano, A. E. (1999). Rigorous model and experimental verification of the radiation field in a flat plate solar collector simulator employed for photocatalytic reactions. *Chemical Engineering Science*, *54*, 2817.

Cabrera, M. I., Alfano, O. M., & Cassano, A. E. (1997). Photocatalytic reactions involving hydroxil radical attack II: kinetics of the decomposition of trichloroethylene using titanium dioxide. *Journal of Catalysis*, *172*, 380.

Coulson, J. M., Richardson, J. F., Backhurst, J. R., & Harker, J. H. (1978). *Chemical Engineering*, Vol. 2, (3rd ed.) (p. 230). Oxford: Pergamon Press.

Gotoh, K. (1977). Morphology of Particle Assemblages, in J. K. Beddow, T. P. Meloy (Eds.), *Advanced Particulate Morphology.* Boca Ratón, FL: CRC Press Inc. p. 171.

Richardson, J. F., & Zaki, W. N. (1954). Sedimentation and fluidisation. part 1. *Transactions of the Institute of Chemical Engineers*, *32*, 35.

Khan, A. R., & Richardson, J. F. (1990). Pressure gradient and friction factor for sedimentation and fluidisation of uniform spheres in liquids. *Chemical Engineering Science*, *45*, 255.

Romero, R. L., Alfano, O. M., & Cassano, A. E. (1997). Cylindrical photocatalytic reactors. Radiation absorption and scattering effects produced by suspended fine particles in an annular space. *Industrial Engineering and Chemical Research*, *36*, 3094.